Systematics of the first 2^+ excitation in spherical nuclei with Skyrme-QRPA

J. Terasaki and J. Engel

Department of Physics and Astronomy,
University of North Carolina, Chapel Hill, NC 27599-3255

G.F. Bertsch

Department of Physics and Institute for Nuclear Theory,
University of Washington, Seattle, WA 98195

Abstract

We use the Quasiparticle Random Phase Approximation (QRPA) and the Skyrme interactions SLy4 and SkM* to systematically calculate energies and transition strengths for the lowest 2^+ state in spherical even-even nuclei. The SkM* functional, applied to 178 spherical nuclei between $Z = 10$ and 90, produces excitation energies that are on average 11% higher than experimental values, with residuals that fluctuate about the average by $-35\% + 55\%$. The predictions of SkM* and SLy4 have significant differences, in part because of differences in the calculated ground state deformations; SkM* performs better in both the average and dispersion of energies. Comparing the QRPA results with those of generator-coordinate-method (GCM) calculations, we find that the QRPA reproduces trends near closed shells better than the GCM, and overpredicts the energies less severely in general. We attribute part of the difference to a deficiency in the way the GCM is implemented.

PACS numbers: 21.10.Pc, 21.60.Jz

I. INTRODUCTION

Computer resources now allow nuclear Density Functional Theory (DFT), also called self-consistent mean field theory, to be applied systematically over the entire nuclear chart. Although it is usually applied to ground states, static DFT can be extended to treat excitations. A number of methods to do so have been developed, and it is not yet clear how accurate any of them is and how they compare to one another. In this paper we apply one of the methods, the Quasiparticle Random Phase Approximation (QRPA), to calculate the properties of the first excited 2^+ states in even-even nuclei. We assess strengths and weaknesses of the method for spherical nuclei and compare results with those of two other systematic studies that used different methods. We have previously carried out QRPA calculations for several isotope chains leading to the neutron drip line [1]; the same theory and codes are used here to cover essentially all known lowest-lying 2^+ states in spherical nuclei.

Among the extensions of static DFT, the QRPA is one of the best justified theoretically. It is the adiabatic limit of time-dependent DFT and as such may be derived from a variational principle. Time-dependent DFT preserves dynamical conservation laws, and in the adiabatic approximation is unambiguously defined by the density functional used for the static properties. Its major shortcoming as an approximation to many-body dynamics is that it works reliably only when ground state is nearly a single Slater determinant or a BCS-like condensate.

Recently, two other systematic calculations of 2^+ excitations that use very different approximation schemes [2, 3] have appeared. Both of these studies constrain DFT by applying external quadrupole fields. This allows one to build a multi-configurational wave function or construct a collective potential-energy surface in deformation space. Reference [2], using the SLy4 energy-density functional [4], treats many constrained configurations together to make a discrete-basis Hill-Wheeler approximation. Reference [3], using the Gogny interaction [5] constructs a collective Hamiltonian in the 5-dimensional quadrupole-deformation space via the collective potential energy surface and a local treatment of the kinetic energy operator. We will refer to both as Generator-Coordinate Method (GCM) calculations.

In addition to the approximation scheme, the quality of the energy-density functional also affects accuracy; most functionals are constructed to optimize their static properties. In this study we cannot hope to make better functional, but we can at least compare the quality of those that already exist. Here we will test two Skyrme functionals, SLy4 [4], and SkM* [6], both in conjunction with "volume" pairing interactions. The results for SLy4 can be directly compared to those of Ref. [2], which uses the same functional[1]. We should note that a relativistic functional has already been applied in the QRPA to a subset of the nuclei we examine here [7].

II. IMPLEMENTATION OF QRPA

Our QRPA and underlying Hartree-Fock-Bogoliubov (HFB) calculations assume spherical symmetry and employ a radial mesh with box boundary conditions. The HFB orbitals are calculated with a code based on the one described in Ref. [8]. For the global survey here, we

[1] In our previous work we also considered the SkP functional [8], but found that under certain conditions it lacks a true variational minimum [9].

give the box a radius of 16 fm and a radial mesh size of 0.05 fm. Although we can take the ordinary DFT functional from mass fits in the literature, the choice of a pairing functional is less clear cut. We have chosen to treat pairing through an ordinary contact interaction, $-V_0\,\delta(\mathbf{r}_1 - \mathbf{r}_2)$. After truncating the space of single-particle orbits (see below), we make an approximate fit of the pairing strength to experimental data. The quantities compared are the average HFB pairing gap [10] and the 3-point difference $\Delta^{(3)}$ of the experimental binding energies. The estimated strengths with the SLy4 functional are $V_0 = 200$ MeV fm^3 for neutrons and $V_0 = 240$ MeV fm^3 for protons [2].

We use the matrix representation of the QRPA in a two-quasiparticle basis, as described in detail in Ref. [12]. We represent the HFB eigenfunctions in the canonical basis, and truncate them through limits on the occupation number (v^2) or, if the pairing gap is zero, on the single-quasiparticle energy [12]. We then construct the usual A and B matrices [13] in the truncated two-quasiparticle basis.

The method was applied to the Ca, Ni, and Sn isotopes for 0^+, 1^-, and 2^+ states in Ref. [1]. In this paper we apply the QRPA to many more nuclei than in Ref. [1], but only consider the low-lying 2^+ states. Unlike the 0^+ and 1^- excitations, the 2^+ states are not affected by spurious modes in spherical nuclei; we can therefore afford to use a smaller space. In our prior work, for example, we used a box radius of at least 20 fm. Here we reduce the radius because the lowest 2^+ states are well localized, even near the drip line. Because we do not have to be as careful about translational symmetry, we reduce the quasiparticle-energy cutoff in the HFB calculation from 200 MeV to 50 MeV. Finally, we increase the canonical-basis occupation-number cutoff — the smallest occupation number that canonical states included in the QRPA can have — from 10^{-8} to 10^{-7}, and reduce the single-particle-energy cutoffs (used when pairing is absent) from 100 MeV to 30 MeV. The only way in which we must extend the basis is by increasing the cutoff in the single-particle angular momentum from 21/2 (in our previous work) to 25/2. The reason is that we are dealing with heavier nuclei here. With all of these limits in place, our largest QRPA matrix, which we encountered in the very heavy nucleus ^{220}Th, has dimension 6086. The space defined by all the cutoffs is large enough so that energies and $B(E2)\uparrow$ strengths do not change when we make it larger still. With the space size fixed, we then determine the strength V_0 of the pairing interaction as described above.

III. SELECTION OF NUCLEI AND THEIR QRPA EIGENMODES

Our goal is to evaluate the performance of the QRPA in all the spherical nuclei with $10 \le Z \le 90$ for which experimental data have been tabulated in Ref. [14]. That reference reports 507 nuclei with measured 2^+ excited states. We select spherical nuclei as follows: We use the HFB code ev8 [15] to do constrained calculations on a grid of deformations, and drop the cases in which the lowest-energy configuration has nonzero deformation. For the remainder, we perform unconstrained calculations, starting from deformation values Q= 0 and $\pm$200 fm^2. If any of these configurations evolves to a lower energy than the spherical one, we drop the nucleus.

[2] The finding that the extracted proton pairing strength is larger than the neutron value appears in other studies as well, e.g. Ref. [11]. The strengths for the SkM* functional are $V_0 = 170$ MeV-fm^3 for neutrons and $V_0 = 200$ MeV-fm^3 for protons.

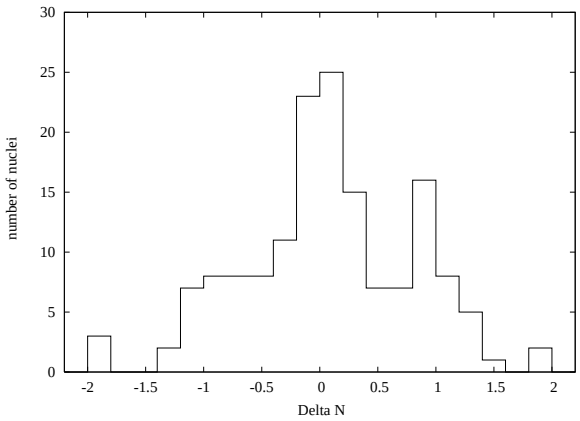

FIG. 1: Particle-hole character of the lowest 2^+ solutions. The histogram displays the quantity ΔN defined in Eq. (1) for 155 nuclei in the SLy4 data set (one of which we drop — see text). The values $-2, 0, +2$ correspond to excitations of hole-hole, particle-hole, and particle-particle character, respectively.

A final requirement for selection is that the QRPA eigenvector correspond to a physical excitation. Thus, we exclude two nuclei in the SLy4 data because the eigenvalues are imaginary[3]. Other unphysical excitations are eigenvectors whose predominant components correspond to pair addition or removal, rather than excitation of the ground state. These components are present because the HFB quasiparticle vacuum does not have a well-defined number of particles. We exclude eigenvectors that have nearly pure two-particle-transfer character, using as a measure an approximate difference in particle number between the ground and excited states:

$$\Delta N = 2 \sum_{ij} (X_{ij}^2 - Y_{ij}^2)(1 - v_i^2 - v_j^2) \,. \tag{1}$$

Here v^2 is a canonical-basis condensate occupation probability, i, j label the quasiparticles in the two-quasiparticle basis, and X, Y are the usual QRPA amplitudes. If $|\Delta N|$ is large, we select another excitation or drop the nucleus from the table altogether. The final tables contain 155 spherical nuclei for the SLy4 functional and 178 for the SkM* functional. We note that the two tables have 129 out of a possible 155 nuclei in common. The imperfect overlap indicates that sphericity is not a very robust property of the DFT, unlike strong deformation. The data sets are posted with the calculated excitation properties in Ref. [16].

Figure 1 shows a histogram of values of ΔN for the SLy4 data set. There is a well-defined peak at $\Delta N = 0$ with a spread of ± 0.4. Beyond that, a plateau covers the range ± 1.3. All these nuclei are included in the data set. Finally, there are 5 transitions that are clearly at the two-particle transfer limit $\Delta N \approx \pm 2$. These nuclei are ^{40,48}Ca, ^{68}Ni, ^{80}Zr, and ^{132}Sn. For all but one (^{40}Ca), an acceptable transition is present at an energy slightly higher than that of the lowest-energy solution and the nucleus is included in our survey.

[3] In principle, the stability of the spherical ground state demands that the eigenvalues all be real. However, the difference between the ways we truncate the HFB and QRPA calculations gives rise to occasional violations.

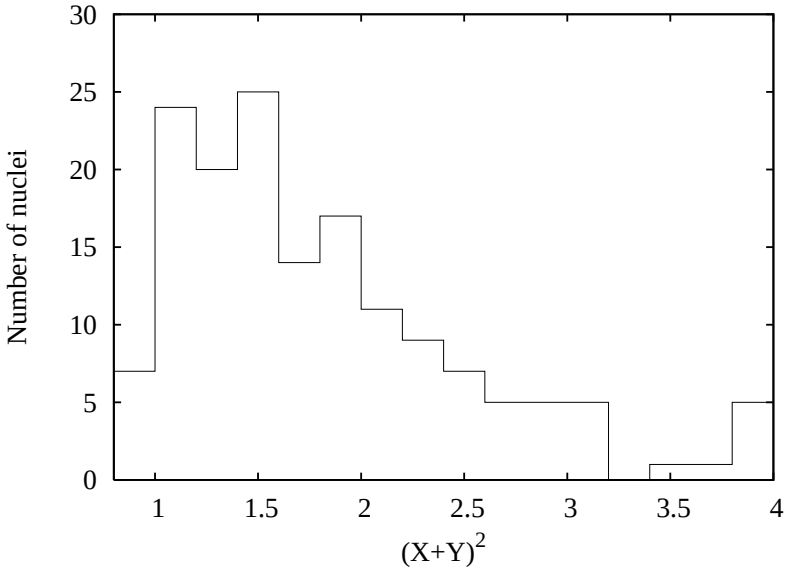

FIG. 2: Distribution of the summed $(X+Y)^2$ amplitudes, Eq. (2), for the first 2^+ transitions in spherical nuclei,for the SLy4 functional. Values greater than 4 are consolidated in the last bin.

We will also want to examine how well the QRPA handles "soft" nuclei, i.e. those which make large excursions from the sphericity. The size of the Y amplitudes is a good measure of softness. The enhancement of T-even transition rates due to the added ground state QRPA correlations is given roughly by the softness parameter

$$C = \sum_{ij} (X_{ij} + Y_{ij})^2. \tag{2}$$

This expression is designed to reduce to unity in the absence of the Y amplitudes and have the basic $(X+Y)^2$ structure characteristic of QRPA transition rates. A histogram for C appears in Figure 2. The softness factors range from 1 (no softness) to more than 4. Even the values in the middle of the histogram would make the Quasiparticle Tamm-Dancoff Approximation invalid. The QRPA itself can have problems with very soft nuclei; if the Y amplitudes are comparable in size with the X amplitudes, then a phase transition to a ground-state of totally different character is nearby.

IV. ENERGIES

Figure 3 shows our predicted energies for the lowest 2^+ states with the SLy4 functional; the predictions are plotted versus measured energies. The data span a range of more than an order of magnitude and the theory captures much of that variation. There are some cases where the errors are very large, however. Far off the line on the upper left hand side are nuclei with $N = 40, Z = 34 - 40$, shown by triangles. They are predicted to be spherical by the SLy4 functional but experimentally they appear to be deformed. On the lower side of the diagonal, the outlying cases are the isotopes of Sn ($Z = 50$) with neutron numbers $N = 60, 62, 64$ (inverted triangles). In this case, the SLy4 functional predicts the nuclei to be very soft with respect to quadrupole deformation. In fact, these 3 nuclei have the highest values of the softness parameter in the data set.

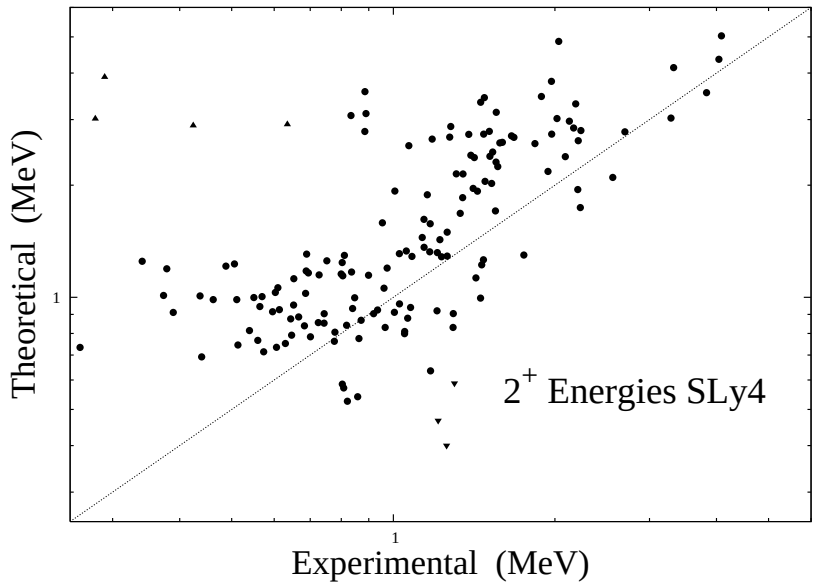

FIG. 3: Calculated energies for lowest 2^+ states in spherical nuclei, plotted versus experimental energies. The theoretical energies are from QRPA with the SLy4 energy functional. The experimental data are from Ref. [14]. For triangles, see text.

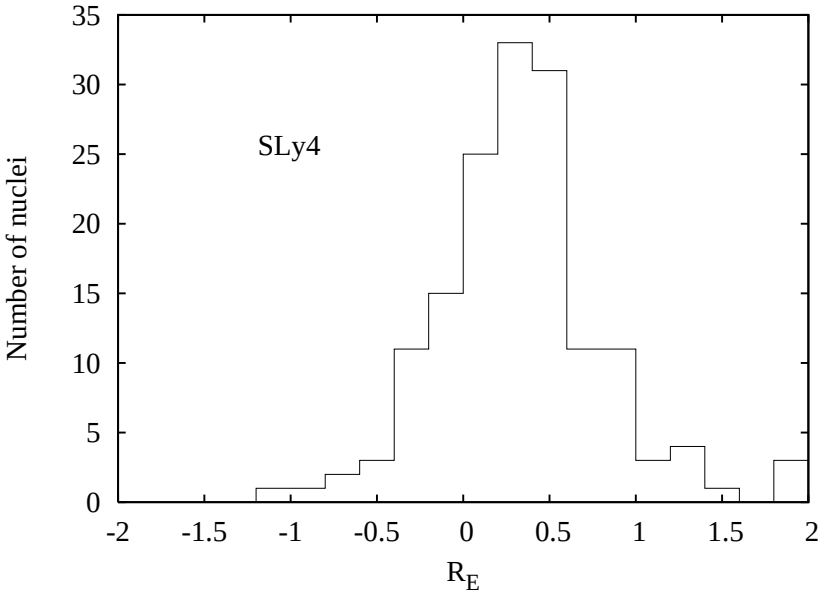

FIG. 4: Histogram of the quantity R_E for the 155 nuclei in the SLy4 data set. The highest bin includes 3 nuclei having $R_E > 2$.

We can quantify the performance of calculations through the measure

$$R_E \equiv \ln(E_{\rm calc.}/E_{\rm exp.})\,, \tag{3}$$

as is done in Ref. [2]. Figure 4 shows a histogram of R_E for the 155 nuclei in the SLy4 data set. We see that theory tends to overpredict the excitation energy, but the error is systematic and the overall distribution is strongly peaked. To summarize performance in

a single number, we can use the average $\bar{R}_E$ for the data set. For spherical SLy4 nuclei, $\bar{R}_E = 0.33$, corresponding to a calculated energy about 40% higher than the experimental value. Another indicator of theory's performance is the width of the peak in the histogram. We define the dispersion of R_E about the average as

$$\sigma_E = \sqrt{\langle R_E^2 \rangle - \bar{R}_E^2}\,. \tag{4}$$

A small value of σ_E implies that the theory tracks fluctuations in the data (though the average is not necessarily correct). For SLy4, the dispersion is $\sigma_E = 0.51$, corresponding to error bars of $+66/-40$ % in the energies. It should be noted that the peak is far from Gaussian, and the bounds $\pm\sigma_E$ include more of the data set than would be the case for a Gaussian distribution. If we were to use the fraction of nuclei inside the bounds to define σ_E, its value would be 20% lower.

It is interesting to see whether the accuracy of the energy prediction depends on other characteristics of the state. To examine this question, we use the value $|\Delta N|$ to split the data set into two parts. Dividing the data set at $|\Delta N| = 0.5$ gives two roughly equal-size subsets. Table I shows the performance measures for the two subsets, and for reference the combined results discussed in the last paragraph. Performance in the high-$|\Delta N|$ set is slightly poorer for both the average and the dispersion, but in our opinion, the differences are not large enough to warrant the use of $|\Delta N|$ as a selection criterion beyond the most extreme cases. We also checked the dependence of accuracy on softness, dividing the data into subsets with C greater and less than 2. The results appear in lines 4 and 5 of the table. The separation strongly affects the averages, so that the high-softness set is actually more accurately described, but the dispersions are not significantly different. It is not totally surprising that states in soft nuclei are better described, as long as the nuclei are not too soft, because such states tend also to be more collective and RPA methods capture collectivity well.

We next examine the performance of the SkM* functional. Here the protocol for selecting spherical nuclei gives a data set with 178 members. The set does not include the nuclei near ^{80}Zr whose energies were poorly predicted by the SLy4 functional. Figure 5 shows the scatter

TABLE I: Averages $\overline{R}_E$ and standard deviations σ_E for measured 2^+ excitations with the SLy4 and SkM* functionals and various cuts on the data set. The set labeled "common" consists of the nuclei that are spherical for both the SLy4 and the SkM* functionals.

functional	data set	Number of nuclei	$\overline{R}_E$	σ_E
SLy4	all spherical	155	0.33	0.51
	low $\|\Delta N\|$	79	0.29	0.47
	high $\|\Delta N\|$	78	0.38	0.54
	low softness	106	0.47	0.48
	high softness	49	0.04	0.44
	common	129	0.26	0.40
SkM*	all spherical	178	0.11	0.44
	low softness	115	0.27	0.35
	high softness	63	−0.17	0.45
	common	129	0.14	0.38

plot of theoretical versus experimental excitation energies. There is more clustering along the diagonal than for SLy4, but outliers still exist on the lower side of the plot. These are all open-shell nuclei, and it is not as easy to characterize them as it was for SLy4. The worst cases are the nuclei ^{44}Ar, ^{64}Zn, and ^{216}Th, shown as the inverted triangles in the figure. What they have in common is a very high QRPA softness, in the range $C = 2 - 8$.

The R metrics for the SkM* data set are given on line 7 of the Table. The average is much better (lower both in the high- and low-softness set) than with SLy4, and there is also some improvement in the dispersion. Much of the improvement comes undoubtedly from the better selection of spherical nuclei, but part may be due to differences in the effective QRPA interaction that comes from the functional. One way to test that is to compare the performance on the 129 nuclei that the two data sets have in common. The results are labeled "common" in Table I. The averages still differ significantly — $\bar{R}_E(\mathrm{SLy4}) - \bar{R}_E(\mathrm{SkM}^*) = 0.12$ — indicating that the functional plays a role beyond merely shaping the ground state. It remains to characterize the aspects of the functional that are responsible, but this is beyond the scope of our project here.

The small-amplitude assumption of QRPA is best justified in magic and semimagic nuclei. Figures 6 and 7 show the very accurate QRPA results with SkM* in the vicinity of doubly magic nuclei in several isotope and isotone chains. Going from left to right in the figures, the magic numbers are $(N, Z) = (28, 20), (28, 28), (40, 28), (50, 40), (82, 50)$, and $(126, 82)$. This last doubly magic nucleus is the one with the highest 2^+ energy in all the chains. We obtain accurate results around doubly magic nuclei with SLy4 as well.

V. TRANSITION STRENGTHS

The $0^+ \rightarrow 2^+$ transition strength for 88 of the 155 nuclei in the SLy4 spherical data set have been measured, and are compiled in Ref. [14]. Figure 8 shows a scatter plot comparing the SLy4 predictions of $B(E2)\uparrow$ with the experimental numbers. Four nuclei for which the

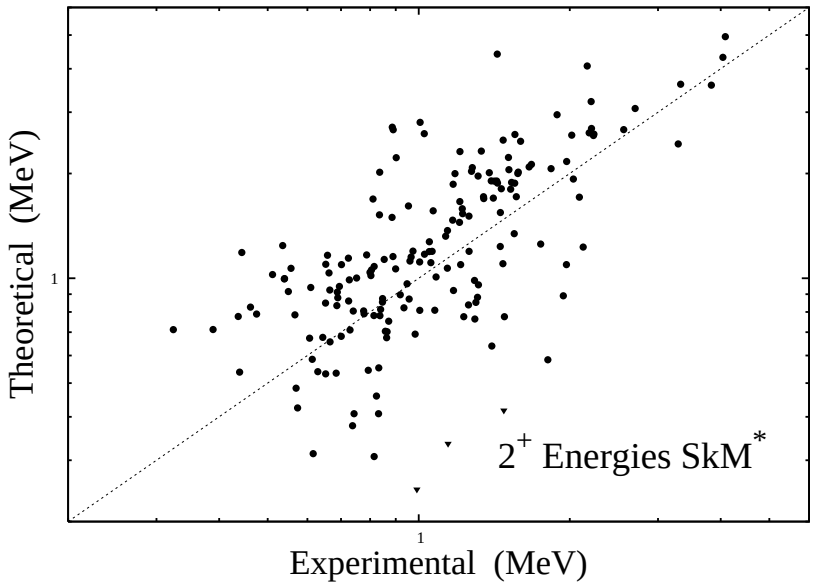

FIG. 5: Same as Figure 3, using the SkM* functional for the calculated energies.

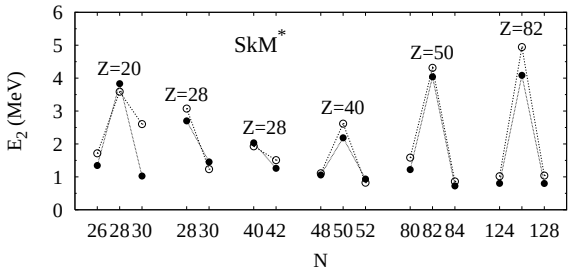

FIG. 6: 2^+ excitation energies in the vicinity of doubly magic nuclei. Displayed on either side of the doubly magic nucleus (N, Z) are the adjacent even-even isotopes, $(N-2, Z)$ and $(N+2, Z)$. Theoretical energies (open circles) were calculated with the SkM* functional. Filled circles are experimental energies.

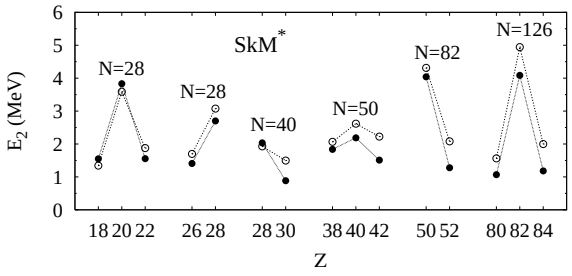

FIG. 7: Same as Figure 6 for isotones $(N, Z-2)$, $(N, Z+2)$ adjacent to doubly magic nuclei (N, Z).

theory seriously underpredicts the data are marked by triangles on the lower side of the scatter plot. The nuclei are ^{38}Ca, ^{34}Ar, ^{42}Ca, and ^{78}Sr, going from left to right on the plot. The nucleus ^{78}Sr is in the deformed $(N, Z) \sim (40, 40)$ region; its large experimental transition strength confirms its deformed character. The failure of the theory for the Ca isotopes near $N = 20$ can be explained by the absence in our calculation of deformed intruder orbits. Only one nucleus on the list, ^{34}Ar, does not have any obvious properties that would cause the QRPA to fail.

On the upper side of the plot, we have marked the most prominent outlier, the nucleus ^{210}Po. Its measured strength is nearly an order of magnitude smaller than the calculated values for both the SLy4 and the SkM* functionals. This discrepancy is one of the most puzzling in the survey, because deformation effects would only increase the transition strength. The predominant amplitude in the transition, with 93% of the normalization sum $\sum X^2 - Y^2 = 1$, has both quasiparticles in the lowest $h_{9/2}$ states, corresponding to the shell-model transition $(h_{9/2}\, h_{9/2})^{J=0} \rightarrow (h_{9/2}\, h_{9/2})^{J=2}$. By itself, the pure shell-model transition has a strength of 454 e^{2}fm^4. The additional small X amplitudes[4] in the QRPA increase the strength by factor of 3.4. An enhancement of the single-particle strength, often represented by effective shell-model charges, is nearly universal in quadrupole transitions. The nucleus ^{210}Po is an exception, with a measured value 200 e^{2}fm^4, even smaller than the shell-model result with bare charges.

To summarize the performance of the QRPA for transition strengths, we follow Ref. [2]

[4] The Y amplitudes play a minor role; the softness parameter C in Eq. (2) is close to unity ($C = 1.09$).

TABLE II: Averages $\overline{R}_Q$ and standard deviations σ_Q of the distributions in R_Q for the SLy4 and SkM* functionals.

functional	$\overline{R}_Q$	σ_Q
SLy4	-0.32	0.42
SkM*	-0.29	0.53

and define the residual of the transition matrix element logarithm R_Q:

$$R_Q \equiv \ln\left[\sqrt{B(E2)\uparrow_{\text{calc.}} / B(E2)\uparrow_{\text{exp.}}}\right] . \tag{5}$$

Figure 9 shows a histogram of this quantity for the SLy4 functional. ^{210}Po on the right clearly stands out as an anomalous case. The long tail on the left represents mainly deformed nuclei that are incorrectly predicted to be spherical. The average and standard deviations of R_Q for both functionals are given in Table II. There is very little difference between the performance of the two functionals when it comes to transitions.

VI. COMPARISON WITH GCM CALCULATIONS

We refer to the GCM-based techniques of Refs. [2] and [3] as GCM-Hill-Wheeler (GCM-HW) and GCM-5-Dimensional-Collective-Hamiltonian (GCM-5DCH) respectively. The

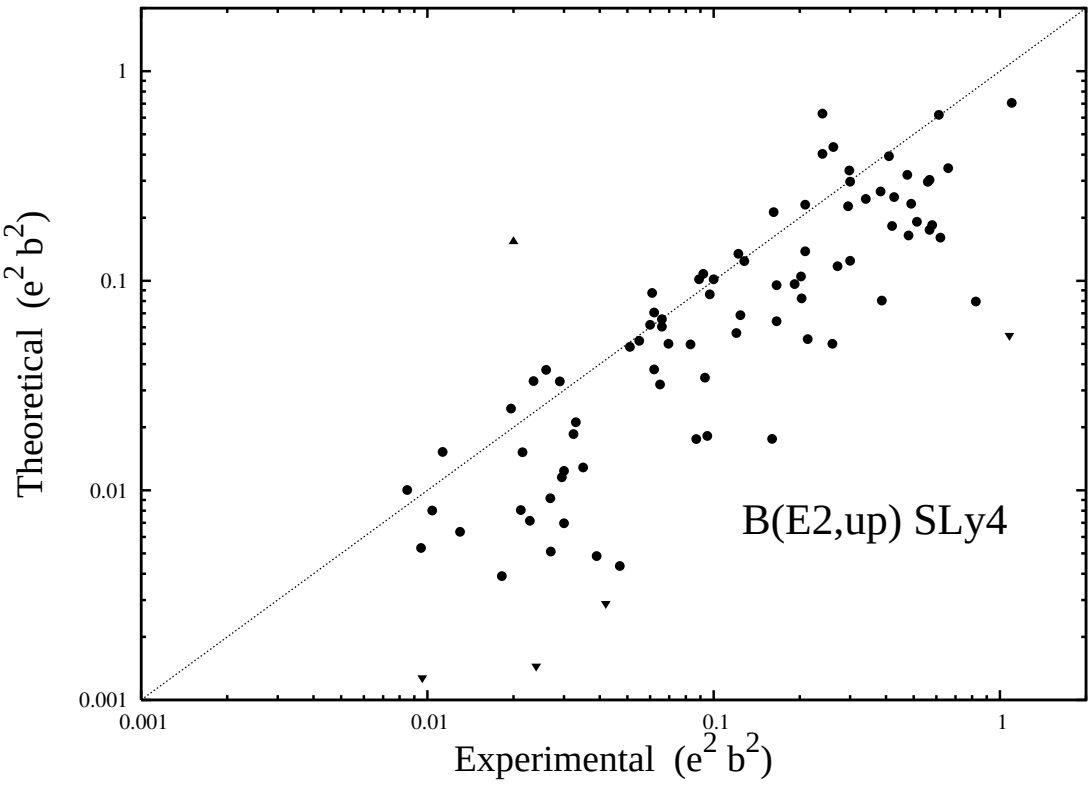

FIG. 8: The same as Figure 3 but for $B(E2)\uparrow$.

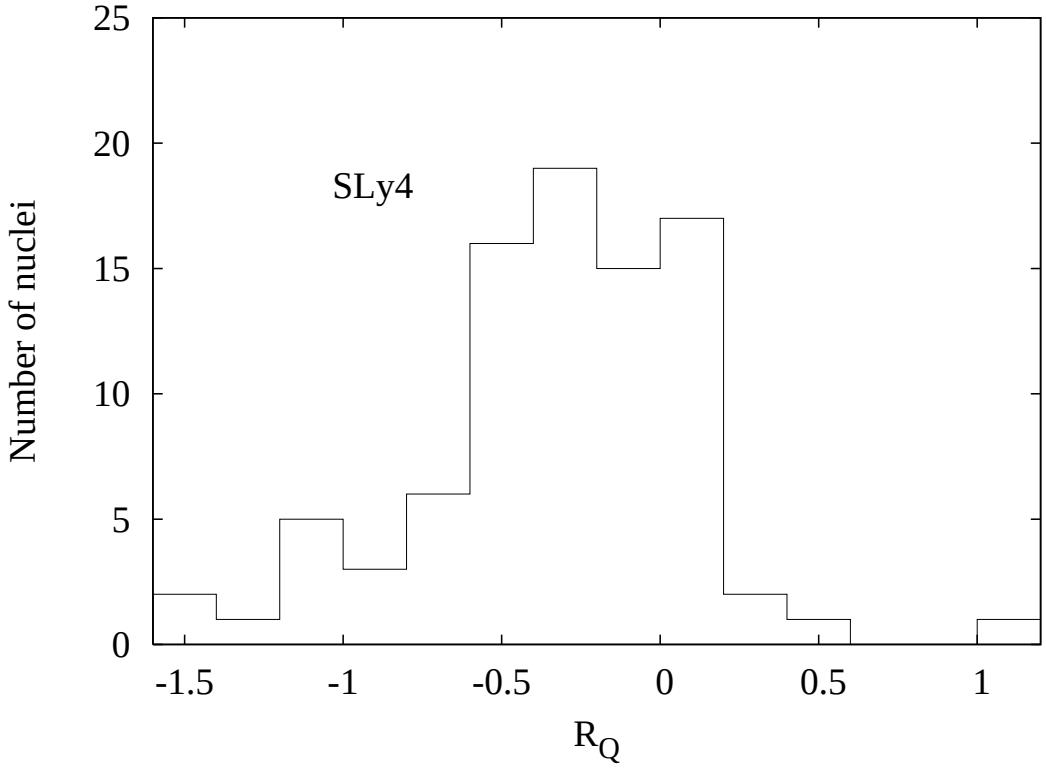

FIG. 9: Histogram of R_Q for the 155 nuclei in the SLy4 data set. The highest bin represents the nucleus ^{210}Po.

GCM-HW study is in some ways the most like ours. It used the SLy4 functional, making the results directly comparable to our SLy4 results. And unlike the GCM-5DCH, it was applied to doubly magic nuclei. Its set of spherical nuclei is somewhat different from ours because of differing pairing interactions, so we use overlap of the two sets for comparison.

The results are in Table III. The energy measures show some interesting differences. From the R_E values we see that the GCM-HW gives energies about 40% higher than those of the QRPA. A possible explanation for the overprediction of energies by the GCM-HW in spherical nuclei appears in the Appendix A. The other interesting difference, which we cannot explain, is that the GCM-HW fluctuations track the experimental ones better than the QRPA.

The $B(E2)\uparrow$ metrics appear in the last two columns of the table. While the QRPA seriously underpredicts the transition strengths, the GCM-HW errs in the opposite direction. It is not surprising that the GCM wave function produces larger quadrupole matrix elements because it incorporates large deformation (unlike the QRPA), and because the $J = 0$ and $J = 2$ states have a similar intrinsic structure.

Unfortunately, because Ref. [3] used a different functional, it is more difficult to compare with our study; it is not possible to distinguish effects of the functional from those of the methodologies. We compare results nevertheless. As before, we use spherical nuclei analyzed in both studies to compute the R-statistics; doubly magic nuclei are thereby excluded. We show in the first line of Table IV the R-statistics of the QRPA with our better-performing functional, SkM*; in the second line are the results from Ref. [3] for the Gogny functional. We see that the QRPA (SkM*) has a somewhat better average energy. On the other hand,

TABLE III: Averages $\overline{R}_E$ and standard deviations σ_E for 153 2^+ excitations produced with the SLy4 functional by our QRPA calculations and the GCM-HW calculations [2].

theory	$\overline{R}_E$	σ_E	$\overline{R}_Q$	σ_Q
QRPA	0.33	0.51	-0.32	0.42
GCM-HW	0.67	0.33	0.16	0.41

TABLE IV: Same as Table III, with the SkM* functional for the QRPA and the Gogny functional for the GCM-5DCH.

theory	$\overline{R}_E$	σ_E	$\overline{R}_Q$	σ_Q
QRPA (SkM*)	0.10	0.45	-0.29	0.51
GCM-5DCH (Gogny)	0.19	0.43	0.22	0.27

the fluctuation of the transition matrix elements is much better described by the GCM-5DCH (Gogny) treatment.

We turn finally to semimagic isotope chains. In Figure 10 we show of our predictions (SkM*) and those of Ref. [3] (along with experimental data) for energies along 3 isotopic chains — $Z = 28$, 50, and 82 — and isotonic chains with the same magic numbers. Here our calculation is again systematically better than that of Ref. [2], the results of which we omit from the plot for the sake of clarity. Our calculation and the GCM-5DCH calculation of

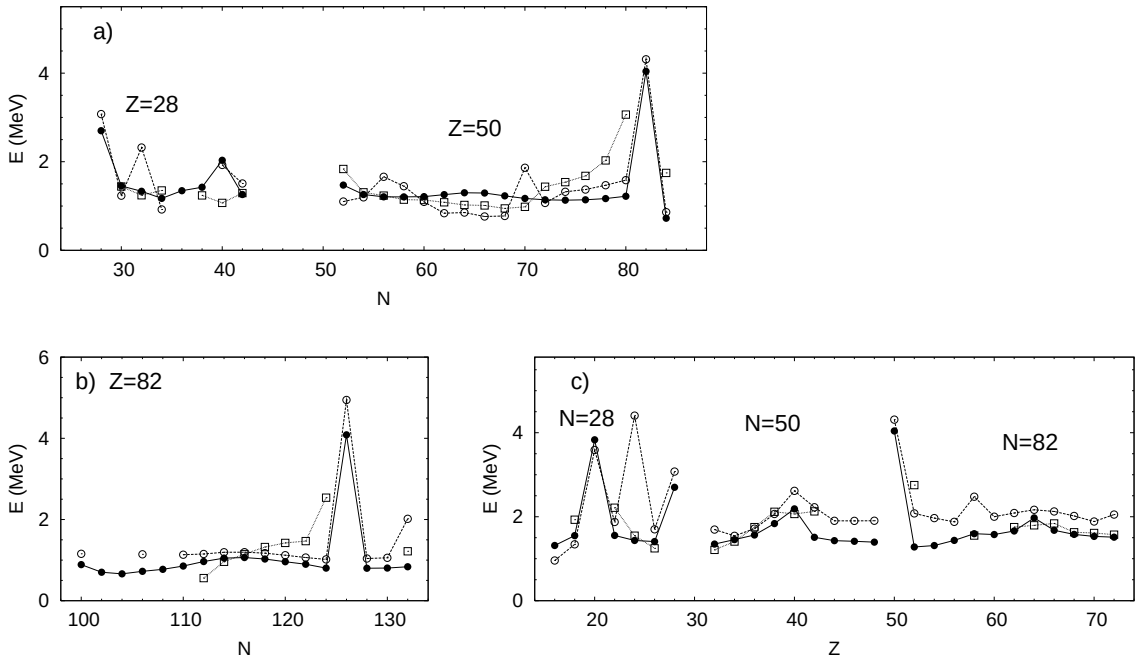

FIG. 10: The lowest 2^+ energies of even Ni, Sn, and Pb isotopes (panels a and b), and isotones with $N = 28$, 50, and 82 (panel c). The open circles represent our results (SkM*), the squares the GCM-5DCH results of Ref. [3], and the filled circles experimental data.

Ref. [3] have complementary virtues in the isotopic chains. The nearly unchanging energies for $Z = 50$ ($52 \leq N \leq 80$) and $Z = 82$ ($112 \leq N \leq 124$), used to motivate the idea of generalized seniority [17], have long challenged mean-field-based approaches. In $Z = 50$, for example, the GCM-5DCH reproduces this trend quite well up to $N = 70$, but then incorrectly predicts a gradual increase in excitation energy as the closed shell at $N = 82$ is approached. Our calculation, by contrast, produces lower energies than experiment around $N = 62$ because the QRPA solutions are close to a transition to quadrupole deformation, but accurately reproduces the sharp jump at $N = 82$. In the $Z = 82$ chain we reproduce the energies well for $112 \leq N \leq 124$, a bit better than does the GCM-HW, particularly near the closed shell. In the isotonic chains, by contrast, the results of the GCM-HW are pretty uniformly better than ours. Again, we cannot be sure how much of the difference is due to functionals and how much to methodology. Ref. [7], which uses a relativistic functional to examine some of these same chains in the QRPA, obtains results that appear comparable to ours.

VII. CONCLUSION

We have used the QRPA to calculate the energies and E2 strengths of the lowest 2^+ states in a wide range of even-even spherical nuclei, and compared the results with experiment for more than 150 energies and more than 80 strengths. We applied two functionals, SLy4 and SkM*. On the whole, SkM* performed better than SLy4. For energies, our calculation with SkM* is comparable to the GCM-5DCH calculation of Ref. [3] in spherical nuclei — better near closed shells, though perhaps not quite as good at midshell — and better than the GCM-HW calculation of Ref. [2]. For $B(E2)\uparrow$ values, the GCM-5DCH calculations appear to be the best if doubly-magic nuclei are excluded. The QRPA is a small amplitude approximation, and its results are not disappointing, considering that limitation.

We were surprised to find that the two functionals disagreed significantly on the question of which nuclei are spherical, an issue that arises at the mean-field level and has nothing to do with the QRPA. We plan to broaden our study soon to include deformed nuclei, allowing a more comprehensive comparison of approaches and functionals.

VIII. ACKNOWLEDGMENT

We thank A. Bulgac for discussions. This work was supported by the UNEDF SciDAC Collaboration under DOE grant DE-FC02-07ER41457. We used computers at the National Energy Research Scientific Computing Center at Lawrence Berkeley National Laboratory.

APPENDIX A: THE RPA AND THE GCM

In this appendix, we present a simple model that indicates why the GCM overpredicts the energy of the lowest 2^+ excitation under conditions for which the RPA works well. The effect of the constraining field Q on the mean-field ground state $|0\rangle$ can be expressed in perturbations theory (that is, for small deformation) as

$$|q\rangle = |0\rangle - \sum_i \frac{|i\rangle\langle i|Q|0\rangle}{E_i} \tag{A1}$$

where $|0\rangle$ is the spherical static-DFT state, $|i\rangle$ the RPA eigenstate, and E_i the corresponding RPA energy. In the GCH-HW approach, one first determines the polarized state $|q\rangle$. The state is then projected so as to have a well-defined angular momentum. The excitation energy is taken to be the expectation value of the Hamiltonian in the projected state. In Eq. (A1), the projection eliminates $|0\rangle$ but keeps the relative amplitudes of the excited components in the above wave function. The expectation value of the Hamiltonian is then given by

$$\langle E\rangle_Q = \frac{\sum_i \frac{\langle i|Q|0\rangle^2}{E_i}}{\sum_i \frac{\langle i|Q|0\rangle^2}{E_i^2}} \tag{A2}$$

To get a quantitative estimate of error in the GCM-HW energy in this small-amplitude limit, we make a two-state approximation to the RPA spectrum, which in fact in spherical nuclei is often dominated by two strong transitions: an in-shell transition at a few MeV or less and the giant isovector quadrupole resonance at 10−15 MeV. The properties we need are their transition strengths and the ratio of their energies $r = E_1/E_2$. It is convenient to express the transition strengths as a fraction of the energy-weighted sum rule:

$$f_i = \frac{E_i\langle 0|Q|i\rangle^2}{\sum_j E_j\langle 0|Q|j\rangle^2}\,. \tag{A3}$$

With some simple algebra the energy expectation value $\langle E\rangle_Q$ can be written in terms of the lowest RPA energy E_1 as

$$\langle E\rangle_Q = E_1\left(\frac{f_1 + (1-f_1)r^2}{f_1 + (1-f_1)r^3}\right) \tag{A4}$$

The right hand side approaches the correct value ($= E_1$) as $r \to 0$.

One case for which the small amplitude approximation (and therefore the RPA) should work well is the doubly magic nucleus ^{208}Pb. In our QRPA calculation with the SLy4 functional, we find an excitation energy of 5.0 MeV with a transition strength that amounts to 17% of the isoscalar sum rule. The giant resonance is located at $E_2 \approx 12$ MeV, giving $r \approx 0.4$. Inserting these numbers in Eq. (A4) results in a GCM-HW energy that is 37% too large, and is close to the value obtained in Ref. [2], $E_2(\mathrm{GCM}) = 6.8$ MeV. This nucleus and others near closed shells, it should be noted, are not good ones for the GCM because of the size of r. Away from doubly magic nuclei r is smaller, resulting in a smaller GCM error for a given f_1.

It might be possible to improve the GCM by adding an additional quadrupole field that would distinguish the giant resonance from the low-lying collective states.

APPENDIX B: SUM-RULE FRACTION

It has been known for a long time that the 2^+ excitation energies and the associated $B(E2)\uparrow$ values have a strong inverse correlation[18], and it is interesting to see how well the theoretical results reproduce this behavior. The product $E_2B(E2)\uparrow$ can be expressed as a fraction of an energy-weighted sum rule, giving it the A-dependence of the sum rule. A form that is often used is $Z^2A^{-\alpha}$, where $\alpha = 1/3$ corresponds to the isoscalar sum rule for a liquid drop[19]. We show in Table V the average of the scaled product

$$S = \frac{E_2B(E2)\uparrow}{Z^2A^{-1/3}} \tag{B1}$$

TABLE V: Average sum rule fraction (Eq. (B1)) and variance

source	data set	Number of nuclei	$\overline{S} = \exp(\overline{R}_S)$	σ_S
experiment	all	328	5.4 10^{-4}	0.46
experiment	spherical	99	4.7 10^{-4}	0.63
DFT	spherical	99	2.8 10^{-4}	0.95

obtained from averaging $R_S = \log(S)$. The variance of R_S is also given in the table. The first line shows the values obtained from the experimental data [14]. The second line contains only the nuclei predicted to be spherical with the SkM* functional. One sees that the average over the spherical nuclei is close to the global average, indicating that the sum-rule fraction is insensitive to deformation. The variance is larger among the spherical nuclei, however. The third line shows the results obtained in the QRPA with the SkM* functional. The theoretical average value is significantly smaller than the empirical value. Since the fraction of the sum rule is a measure of the collectivity, it may be that our functional does not have sufficient collectivity. The sum-rule fraction might be sensitive to the strength of the pairing interaction or some other aspect of the functional, and it would be interesting to investigate that issue further.

The table also shows that the fluctuation in the sum-rule fraction, σ_S, is significantly larger in the DFT calculation than in experiment. Shell structure may need to be suppressed in some way, perhaps by increasing the pairing strength.

[1] J. Terasaki and J. Engel, Phys. Rev. C **74**, 044301 (2006).
[2] B. Sabbey, M. Bender, G. F. Bertsch, and P.-H. Heenen, Phys. Rev C **75**, 044305 (2007).
[3] G. F. Bertsch, M. Girod, S. Hilaire, J.-P. Delaroche, H. Goutte, and S. Péru, Phys. Rev. Lett. **99**, 032502 (2007).
[4] E. Chabanat, P. Bonche, P. Haensel, J. Meyer, and R. Schaeffer, Nucl. Phys. A **635**, 231 (1998).
[5] J. Dechargé and D. Gogny, Phys. Rev. C **21**, 1568 (1980).
[6] J. Bartel, P. Quentin, M. Brack, C. Guet, and H.-B. Håkansson, Nucl. Phys. A **386**, 79 (1982).
[7] A. Ansari and P. Ring, Phys. Rev. C**74** 054313 (2006).
[8] J. Dobaczewski, H. Flocard, J. Treiner, Nucl Phys. A **422** 103 (1984).
[9] T. Lesinski, K. Bennaceur, T. Duguet, and J. Meyer, Phys. Rev. C**74** 044315 (2006).
[10] J. Dobaczewski, W. Nazarewicz, T.R. Werner, et al., Phys. Rev. C**53** 2809 (1996).
[11] S. Goriely, M. Samyn, P.-H. Heenen, J.M. Pearson and F. Tondeur, Phys. Rev. C**66** 024326 (2002).
[12] J. Terasaki, J. Engel, M. Bender, J. Dobaczewski, W. Nazarewicz, and M. Stoitsov, Phys. Rev. C **71**, 034310 (2005).
[13] P. Ring and P. Schuck, *The Nuclear Many-Body Problem* (Springer-Verlag, New York, 1980).
[14] S. Raman, C. W. Nestor Jr., and P. Tikkanen, At. Data Nucl. Data Tables **78**, 1 (2001).
[15] P. Bonche, H. Flocard, and P.-H. Heenen, Comput. Phys. Commun. **171** 49 (2005).
[16] Tables of our results will be placed on the EPAPS server upon publication. They are also available to download from http://unedf.org/qrpa.

[17] I. Talmi, Nucl. Phys. A **172**, 1 (1971).
[18] L. Grodzins, Phys. Lett. **2**, 88 (1962).
[19] A. Bohr and B. Mottelson, Mat. Fys. Medd. Dan. Vid. Selsk. **27** No. 16 (1953).